Bim contributes to the progression of Huntington's disease-associated phenotypes

Sheridan L. Roberts[1, #], Tracey Evans[1,#], Yi Yang[1], Yuhua Fu[2], Robert W. Button[1], Rebecca J. Sipthorpe[1], Katrina Cowan[1], Evelina Valionyte[1], Oleg Anichtchik[1], Huiliang Li[3], Boxun Lu[2,$] and Shouqing Luo[1, *]

1. Peninsula Schools of Medicine and Dentistry, Institute of Translational and Stratified Medicine, University of Plymouth, Research Way, Plymouth PL6 8BU, UK

2. State Key Laboratory of Medical Neurobiology, School of Life Sciences, Fudan University, Shanghai, China, 200438

3. Wolfson Institute for Biomedical Research, University College London, Gower Street, London, WC1E 6BT, UK

[#] These authors contribute equally to this work

[$]Co-senior author

*Correspondence: shouqing.luo@plymouth.ac.uk

Abstract

Huntington's disease (HD) is a neurodegenerative disorder caused by an expanded polyglutamine (polyQ) tract in the huntingtin (HTT) protein. Mutant HTT (mHTT) toxicity is caused by its aggregation/oligomerisation. The striatum is the most vulnerable region, although all brain regions undergo neuronal degeneration in the disease. Here we show that the levels of Bim, a BH3-only protein, are significantly increased in HD human post-mortem and HD mouse striata, correlating with neuronal death. Bim reduction ameliorates mHTT neurotoxicity in HD cells. In the HD mouse model, heterozygous Bim knockout significantly mitigates mHTT accumulation and neuronal death, ameliorating disease-associated phenotypes and lifespan. Therefore, Bim could contribute to the progression of HD.

Introduction

Huntington's disease (HD) is an autosomal-dominant progressive neurodegenerative disease, characterised by movement and cognitive dysfunction (1, 2). HD is caused by an expansion of CAG repeats in the huntingtin (*HTT*) gene encoding an expanded polyglutamine (polyQ) stretch near the N terminus (3), where 36 repeats are considered a pathological threshold. Genetic and transgenic data suggest that the mutation causes the disease predominantly by gain-of-function mechanisms. Mutant HTT (mHTT) is believed to induce neurodegeneration through its aggregation and toxicity. These lead to loss of signaling by brain-derived neurotrophic factor, endoplasmic reticulum stress (4), perturbation of Ca2+ signaling, alterations of gene transcription, inhibition of protein clearance pathways, mitochondrial disturbances, and ultimately cell death (5). However, the mechanisms underlying these critical events are yet poorly understood. In HD, cell death occurs in various brain regions, but striatal medium spiny neurons undergo the greatest degeneration (6).

To date, there is no effective clinical treatment to slow down the disease progression. Given the nature of the toxic gain-of-function from mHTT, which potentially relates to the conformation of expanded polyQ (reviewed in (7)), lowering mHTT that primarily causes the pathogenic processes would be appealing for HD therapeutic intervention (8). Screening studies revealed that mHTT genetic modifiers rescue HD-associated phenotypes (9-13). The human trial of HD using a non-allele specific antisense oligonucleotide (ASO) has gained a success in lowering mHTT (14). Nevertheless, the loss-of-function effect of mHTT, due to wild-type (WT) HTT haploinsufficiency and mHTT aggregation, was also suggested to contribute to HD pathology (15). It is important to reveal the mechanism of disease

progression and identify the pathways/targets that specifically modulate the levels of mutant HTT and neurotoxicity.

Bim, a BH3-only pro-apoptotic protein, is crucial to initiate apoptosis (16), and it is critical for neuronal apoptosis when neurons are induced by endoplasmic reticulum (ER) stress (17) and trophic factor deprivation (18). We identified that Bim negatively regulates autophagy by mislocalising the Beclin 1-Vps34 complex that is essential for autophagy initiation (19). Since Bim regulates both autophagy and apoptosis, targeting Bim would have a dual mechanism of action to mitigate neuronal cell death, given that autophagy is neuroprotective, and apoptosis is pathogenic in neurodegeneration conditions. Previously Bim was shown to be increased in an HD striatal cell line (20), and was proposed to be a potential link between proteasome dysfunction and cell death caused by mHTT (21). Currently, it is unknown whether Bim plays a role in HD progression. Our present data show that the increase of Bim in HD cells and mice correlates with neuronal degeneration. Reduction in Bim levels effectively alleviates the pathology of HD in both *in vitro* and *in vivo* models via reduction in mHTT and neuronal toxicity. These data suggest that Bim contributes to HD-associated phenotype progression.

Results

The increased levels of Bim in human HD and HD-like mouse tissues

Bim is degraded by proteasomes (22), and the ubiquitin proteasome system (UPS) is often perturbed in HD (23, 24). Thus, the levels of Bim proteins may be elevated in HD cell and mouse models (20, 21, 25). We first examined Bim levels in the SK-N-SH neuroblastoma cells expressing expressing GFP control, GFP-HTT exon1-21Q (HTT-21Q) or GFP-HTT

exon1-72Q (HTT-72Q), and confirmed that Bim levels were increased in HTT-72Q-expressing SK-N-SH cells (**Supplementary Material, Fig. S1A**). In these cells, the levels of Bim increase were comparable to those in Bim increase caused by MAPK inhibitor U0126 (**Supplementary Material, Fig. S1A**). Similarly, Bim protein levels were also increased in mouse knock-in HD striatal cells expressing HTT-111Q (STHdhQ111) (**Supplementary Material, Fig. S1B**), compared to the control cells expressing HTT-7Q (SThdhQ7). We further tested if Bim levels were increased in human HD post-mortem striatal tissues. Bim protein levels were significantly increased in human HD post-mortem striatal tissues, compared with those in controls by immunoblot (**Fig. 1A**). We also tested Bim levels in N171-82Q HD mice. The N171-82Q HD transgenic mouse model expresses the first 171 amino acid residues of human HTT with 82Q (N171-82Q) driven by mouse prion promoter, and the transgene almost exclusively displays neuronal expression (26). We confirmed that Bim protein levels were significantly increased in HD mice at multiple ages (**Fig. 1B-C**), while Bim mRNA levels did not undergo a significant change in HD mice of 10-17 weeks, compared to matched WT mice (**Fig. 1D**). Similarly mRNA levels did not significantly increase in HD mice at a younger age of 8 weeks (**Supplementary Material, Fig. S1C)**. This suggests that the elevation of Bim protein may be attributed to a reduction in Bim turnover of HD mice, in comparison to that in WT mice. Using SK-N-SH cells, we confirmed that Bim protein turnover in the cells expressing HTT-72Q was slower than that in the cells expressing HTT-21Q (**Supplementary Material, Fig. S1D**). Interestingly, among Bcl-2 family or cell death-related protein, Bim underwent the maximal change in HD mice (**Fig. 1E**). Notably, the relative levels of Bim (over age-matched WT mice) peaked at 12 weeks (**Fig. 1C**). We reason that, upon this point, the neurons with the highest levels of Bim would undergo sharp degeneration, producing lower levels of proteins. As a result, the relative levels of Bim are expected to reduce after the peak time window. Indeed, the neuron marker NeuN levels in the

striatum of HD mice were lower than those in WT mice at 14 weeks (**Supplementary Material, Fig. S1E**), suggesting that neurons were significantly degenerated in HD mice at the age.

Bim reduction alleviates mHTT neurotoxicity

We investigated the potential role of Bim in mHTT toxicity in HD cell models. In SK-N-SH neuroblastoma cells expressing HTT-72Q, Bim levels were increased (**Supplementary Material, Fig. S1A**). Bim knockdown significantly enhanced the viability of SK-N-SH cells expressing HTT-72Q (**Fig. 2A**), suggesting that Bim reduction alleviates HTT-72Q toxicity in the cells. Serum starvation induces cell death in knock-in striatal cells STHdhQ111 that express HTT-111Q (27). Bim levels were also increased in STHdhQ111 striatal cells, compared to those in STHdhQ7 cells (**Supplementary Material, Fig. S1B**), and Bim siRNA knockdown significantly increased cell viability in STHdhQ111 cells in starvation conditions (**Fig. 2B**).

We next aimed to explore if Bim reduction could exert a protective effect against mHTT toxicity *in vivo.* Bim knockout mice do not display any behavioral abnormalities, except that lymphocytes are insensitive to certain apoptotic stimuli (28). While Bim-/- mice have enlarged spleens, as previously reported (28), Bim+/- or HD/Bim+/- mice have normal-sized spleens (**Supplementary Material, Fig. S2**). As such, we aimed to employ HD Bim+/- mice with reduced Bim for our later studies. We tested if Bim reduction could ameliorate neurotoxicity in the HD mouse model. Reduced caspase 3 cleavage shown by western blot further confirmed that apoptosis occurred at a lessened extent in HD Bim+/- mice (**Fig. 2C**). Similarly, Bim reduction significantly ameliorated neuronal cell death that was marked by cleaved caspase 3 (**Fig. 2D**). Toluidine blue staining has been used to monitor

neurodegeneration in mouse brain tissues, and the levels of its staining inversely correlated with neuronal health (29, 30). **Fig. 2E** shows that striatal neurons were less stained in HD Bim+/- mice, compared with those in HD mice. These suggest that neurodegeneration could be weakened in HD mice with reduced Bim protein levels.

Bim reduction ameliorates mHTT aggregation

Using SK-N-SH neuroblastoma cells with mHTT expression, we confirmed that Bim knockdown reduced HTT-72Q aggregation (**Fig. 3A**). Bim knockdown also reduced the levels of HTT-72Q in SK-N-SH cells by immunoblot (**Supplementary Material, Fig. S3A**). We then examined mHTT aggregation *in vivo* in our HD mice. In our conditions, the HD mice typically showed disease phenotypes from 10 weeks. Consistently, mHTT aggregation was significantly ameliorated in HD Bim+/- mice across 10-14 weeks. The levels of mHTT aggregation and the size of mHTT aggregates in HD Bim+/- mice were significantly smaller than that in HD mice at the tested ages (**Fig. 3B**). The levels of mHTT protein were markedly reduced in HD Bim+/- mice (**Fig. 3C**), while WT HTT protein levels did not reduce in HD Bim+/- mice (**Supplementary Material, Fig. S3B**). qPCR assays show that Bim reduction does not reduce human mHTT transgene mRNA levels in HD mice (**Supplementary Material, Fig. S3C**). This suggests that Bim reduction selectively lowers mHTT in the protein level, presumably contributing to alleviation of mHTT toxicity.

Reduction in Bim ameliorates HD-associated phenotypes and increases life expectancy

We tested the effect of Bim reduction on HD-associated behavioural phenotypes in WT, HD or HD Bim+/- mice. Rotarod tests have been widely used for locomotor activity in HD mice (31). From 8 weeks, the latency to fall of HD mice was lower than that of WT mice. In HD mice, the latency to fall sharply dropped at the age of 10 weeks, and further reduced at the

age of 12 weeks. However, in HD Bim+/- mice, the performance during 8-12 weeks was stable and mitigated (**Fig. 4A**). Overall, Bim heterozygous knockout significantly ameliorated the fall latency (**Fig. 4A**). The forelimb and hindlimb muscle strength by the Grip-strength test is usually used as an indicator of neuromuscular function (31, 32). We employed Grip-strength tests to examine the levels of muscle wasting and neuromuscular function, which are considered the early indicators of HD pathology (33). **Figure 4B** shows that Bim reduction delayed the rate at which grip strength declined in HD mice. Using the video tracking software to record and analyse the behaviours of WT, HD and HD Bim+/- mice in an open-field maze, we identified that HD Bim+/- mice performed better than HD mice globally in mean speed (**Fig. 4C**) and distance travelling (**Fig. 4D**) from 6 to 14 weeks. The Novel object recognition test was used to evaluate memory through the comparison between recognition of a previously explored object (familiar) and that of a novel object (34). HD Bim+/- mice showed an improvement in discrimination ratios of visit durations or numbers at the novel objects, which abruptly declined in HD mice at 12-14 weeks of ages (**Fig. 4E-F**). The total exploration (total number of visits to familiar and novel objects) and marble burying are used to depict changes in animal behaviours such as anxiety (35, 36). This assay has also been used as an additional method to measure the motor defects (35). The total exploration numbers (identified in the Novel object recognition test) and Marble burying test showed that Bim reduction in HD Bim+/- mice ameliorated the motility and behaviours that were affected in HD mice across all the tested ages (**Fig. 4G-H**). These data suggest that Bim reduction improves both physical and cognitive performance in HD mice. Of note, Bim reduction did not significantly change the phenotypes of WT or Bim+/- mice in the Rotarod test (**Supplementary Material, Fig. S4A**), the Grip-strength test (**Supplementary Material, Fig. S4B**) or Open-field test (**Supplementary Material, Fig. S4C-D**). Similarly, the exploration and Marble burying tests did not show significant changes in WT and Bim+/- mice

(**Supplementary Material, Fig. S4E-F**). These suggest that Bim reduction selectively improves HD-associated phenotypes. Bim reduction resulted in an extension of the lifespan in HD mice by 15-20% (**Fig. 5A, Supplementary Material, Fig. S5**). The effect of Bim reduction on the life expectancy of HD mice is comparable to that in HD mice treated with Congo red (37) or caspase 1 inhibition (38). Collectively, these data suggest that Bim contributes to the progression of HD-associated phenotypes, and reducing Bim activity would result in the amelioration of cell death, mitigating mHTT toxicity in HD (**Fig. 5B**).

Discussion

The monogenetic inheritance of HD makes the disease a unique model for the studies of neurodegeneration featured with proteotoxicity. The progressive neurodegeneration of HD is a key feature in the disease development. As a BH3-only protein, Bim has long been known to induce apoptosis, playing roles in neuronal death regulation (16, 18). We identified Bim as an autophagy negative regulator by mislocalising Beclin 1 (19, 39). Bim was reported to be increased in HD cell models (20, 21) and in the striata of HD R6/1 mice (25). Yet, it was unknown if the increase in Bim contributes to HD-associated phenotype progression. Here we aimed to address this by using HD cell and mouse models. A number of HD mouse models are currently available to suit various studies of mHTT. In this study, we used the N171-82Q mouse model. The pathological signs of the N171-82Q mice start from 8 weeks and premature death occurs from 16-21 weeks (26). First, the relatively severe phenotype in the mouse model allows us to ascertain the potential improvement in Bim-reduced HD mice. Second, the N171-82Q transgene driven by mouse prion promoter has almost exclusively neuronal expression (26). Therefore, this model maximally avoids mHTT inclusions in peripheral tissues and muscle atrophy, which may affect motor task experiments (such as

Rotarod and Grip-strength tests). Third, our early data show that Bim levels were markedly increased in the N171-82Q mice.

Bim mRNA levels did not appear to undergo a significant change in HD mice, compared to those in WT mice. Our data from cell culture suggest that reduced turnover in Bim protein would be a main cause for the increase of the protein in HD conditions. This is presumably due to mHTT-induced UPS perturbation, as suggested previously (23, 24). Of note, the relative levels of Bim in HD mice (over those in the age-matched WT mice) reduced after 12 weeks. In our conditions, HD mice typically started to die from 13 weeks. At 12 weeks, Bim would accumulate and peak in HD mouse neurons. Upon this point, the neurons, which had the highest levels of Bim, would undergo sharp degeneration, either dying or producing reduced levels of the proteins.

This study provides *in vivo* data suggesting that the increase in Bim protein levels could contribute to the progression of HD-associated phenotypes. Bim reduction improved the defects of multiple phenotypes in HD mice, including fall latency, grip strength, travelling, object discrimination and exploration. The extent of lifespan extension by Bim reduction is similar to that observed in HD mice treated with Congo red treatment or caspase 1 inhibition (37, 38). Notably, the lifespan improvement is relatively mild in HD Bim+/- mice. We assess the following reasons could account for the relative mild effect on the lifespan. First, although Bim reduction decreased neuronal cell death, ameliorating HD pathology, mHTT toxicity was not abolished by Bim reduction. Bim level upregulation is presumably one of multiple key factors that contribute to neuronal apoptotic cell death and the pathology. For example, BNIP3 could also be upregulated in HD mice (**Fig. 1E**), potentially contributing to neuronal death. Second, mHTT could confer the toxicity that is independent of apoptosis. It

has been shown that necroptosis and ferroptosis would also be involved in HD (40, 41). Third, the lifespan in the N171-82Q mice tends to be variable (42). The death in these mice could be partially dependent on the indirect effect of mHTT toxicity, such as starvation due to unwillingness in food intake. In HD mice, phenotype-rescuing effects might not be exactly reflected by the extension in lifespan. We previously reported that rapamycin could rescue HD-associated phenotypes in the N171-82Q mice, however it did not improve the lifespan in the model (31).

We have shown that Bim negatively regulates autophagy by mislocalising the Beclin 1-Vps34 complex that is essential for autophagy initiation (19). Bim reduction indeed lowered mHTT levels. Current studies do not address if autophagy plays a role in mHTT lowering during Bim reduction. Further study would be necessary to examine if the autophagic involvement of Bim upregulation contributes to HD progression.

Materials and Methods

Antibodies and reagents

The indicated antibody dilutions were used for western blot (unless otherwise indicated). Rabbit polyclonal antibodies: anti-Bim (1:1,000) (CST, 2933); anti-p62 (1:3,000) (MBL, PM045); anti-actin (1:1,000) (Sigma, A2066); anti-LC3 (1:1,000) (MBL, PM036); anti-LC3 A/B (1:3,000) (CST, #12741); Bcl-xL (1:1,000) (BD, 556361); BNIP3 (1:1,000) (CST, 44060); caspase 3 (1:1,000) (CST, 9665); active caspase 3 (1:1,000) (CST, 9661); NeurN [EPR12763] (1:1000) (Abcam, ab177487)； Bax (1:1000) (Upstate, 06-499); Bak (1:1000) (Upstate, 06-536); Bid (1:1000) (CST, 2003); Bcl-2 (1:1000) (CST, 2870); AIF (1:1000) (Chemicon International, AB16501). Mouse monoclonal antibodies: anti-GAPDH (1:5,000) (Ambion, AM4300); MW1 (1:200) (DSHB); BAD (1:300) (Santa Cruz, sc-8044); HTT (1:1,000) (Millipore, MAB2166). Cycloheximide (50 µg/ml, C4859) was purchased from Sigma; U0126 (10 µM, Cat No: 662005) was from CalBiochem. GFP-HTT-21Q and GFP-HTT-72Q have been used in our previous studies (43).

Cell culture

SK-N-SH cells were cultured in DMEM containing 10% FBS. STHdh (CH00096-Q111/Q7) cells were obtained from Coriell Cell Respositories. All mammalian cell lines, except STHdh cells, were maintained in an incubator at 37 ^{o}C, with 5% CO_2. STHdh cells were cultured in DMEM containing 10% FBS at 33 ^{o}C, with 5% CO_2. Transfection was performed with Lipofectamine 2000 or 3000 (for SK-N-SH neuroblastoma cells) according to standard methods.

Quantification of mHTT aggregates in cultured cells

To measure mHTT aggregates, approximately 500 GFP-mHTT-positive cells were counted in multiple random visual fields per slide a under fluorescent microscopy. All coverslips were scored with the observer blinded to the identity of the slides. The figures show data from representative experiments in triplicate.

Measurement of mHTT aggregates in brain tissues

Quantification of mHTT aggregate size in mouse brain tissue was performed using the Fiji Image J, 200-500 cells were counted in multiple random visual fields per animal. All coverslips were scored with the observer blinded to the identity of the slides. The scale bar was measured and set per image, followed by the length of the largest aggregate per cell being measured and recorded. The total percentage of nuclei with aggregates greater than 1.5 μm was scored, in addition to average mHTT aggregate size (μm). Cells were imaged at 40x magnification using bright-field microscopy on a Leica IM8. The figures show data from representative experiments in triplicate.

Immunocytochemistry

As previously described (44), cells were fixed with 4% paraformadehyde for 10 min after washing with phosphate-buffered saline (PBS) twice. The fixed cells were washed three times in PBS, then permeabilised with 0.5% Triton in PBS for 10 min. Cells were blocked in blocking buffer (1% BSA, 1% heat inactivated goat serum in PBS) for 30 min at room temperature. Primary antibodies were incubated with cells overnight at 4°C. The secondary antibody was incubated for 30 min after washing three times (10 min, each). Cells were washed three times (10 min, each) after incubation with secondary antibodies, then mounted with Citifluor containing DAPI (1 μg/ml).

Immunoprecipitation

Immunoprecipitation (IP) was performed using Buffer A (20 mM Tris-HCl, pH 7.2, 2 mM $MgCl_2$, 150 mM NaCl, 5 mM NaF, 1 mM Na_3VO_4, 0.5% NP-40, protease inhibitor cocktail [Roche]). Cells were lysed in Buffer A for 20 min on ice, followed by centrifugation at 13,000 x g for 15 min. Primary antibodies (or anti-Flag M2-agarose affinity gel) were added to a final concentration of 5 µg/ml and incubated for 2 hours to overnight at 4°C. Anti-mouse or rabbit IgG agarose were added to the mixture and incubated at 4°C for 1 hour. Following three washings, IP products were boiled in Laemmli buffer, and subjected to PVDF membrane transfer and western blot.

Flow cytometry - cell death assay

Cell death was performed as previously described (43). Trypsinised cells were washed twice with cold PBS and resuspended in 1x binding buffer (10 mM HEPES, pH 7.4; 140 mM NaCl; 2.5 mM $CaCl_2$) at $1x10^6$ cells/ml. 100 µl of these cells were transferred to a FACS tube, treated with 5 µl propidium iodide (Sigma) and incubated for 15 min at room temperature. Each tube had a further 200 µl of 1x binding buffer added and then was analysed by flow cytometry.

SiRNA transfection

HeLa cells were split 1 day prior to transfection to 50% confluence and left overnight in antibiotic-free DMEM containing 10% FBS. In most cases, siRNAs were transfected with Lipofectamine 2000 according to the manufacturer's instructions. TransIT-2020 (Mirus) was used for STHdh cell transfection. The following siRNAs were used for knockdown experiments. Control siRNA (CST): 5'-CGUACGCGGAAUACUUCGA-3'. Non-targeting siRNA was the control siRNA. Human Bim siRNA (CST): 5'-

CAGGGAGACGUGUGAUAUA-3'; mouse Bim siRNA (Eurofin): 5'-GGCUUCCAUACGACAGUCUCA-3' (for STHdh cells).

Cell viability assay

Cell survival was determined with Cell Titer-Glo Luminescent cell viability Assay kit (Promega) to measure ATP levels according to the manufacture's instruction. Briefly, 100 µl of Cell Titer-Glo reagent was added to the culture medium. Cells were placed on a shaker for 5 min and then incubated at room temperature for 10 min. A plate reader was used for Luminescent reading.

Mice breeding and maintenance

The strains of Bim knockout mice (stock# 004525) (28), and WT mice (stock# 000664) were from the Jackson Laboratory. WT mice were crossed with Bim−/− mice to generate Bim+/− mice. Bim+/− mice were crossed with Bim+/− mice to generate Bim−/− mice and Bim+/+. Mice were genotyped by PCR using the following primers. Common: 5'-CATTCTCGTAAGTCCGAGTCT-3'; wild-type: 5'-GTGCTAACTGAAACCAGATTAG-3'; mutant: 5'-CTCAGTCCATTCATCAACAG-3' (according to instructions from the Jackson Laboratory). HD mice expressing HTT N171-82Q (mHTT) (Jackson laboratory, strain: B6C3, Stock #: 003627) (31, 44) were were crossed with our WT stock B6 mice for over 6 generations to clean the background and amplify the clone before crossing the mice with Bim knockout mice. All mice in this study were on a C57BL/6 genetic background.

HD mice were genotyped by PCR using the primers: 5'-GAACTTTCAGCTACCAAGAAAGACCGTGT-3'; 5' GTGGATACCCCCTCCCCCAGCCTAGACC-3'. HD mice were bred with Bim knockout mice. Bim knockout mice exhibit a normal phenotype (except that lymphocytes are

insensitive to certain apoptotic stimuli) and do not display any behavioral abnormalities (45). HD transgenic (HD) mice were bred with Bim+/- mice to achieve Bim +/ + (wild type), Bim +/-, HD Bim+/- and HD Bim+/+ mice. For all experiments age matched littermates were used. All animal work was performed according to UK Home Office legislation and with appropriate licences.

qPCR

Homogenisation of the tissue was undertaken using a syringe and 0.8 mm gauge needle (BD Plastipak) with QIAzol lysis buffer from the miRNAeasy kit (Qiagen) and RNA was isolated according to manufacturer's instruction. For qPCR analysis, 0.48 µg total RNA was reverse transcribed using the High-Capactity, cDNA Reverse Transcription Mix (Applied Biosystems) using cycles of 25°C (10 min), 37°C (120 min) and 85°C (5 min). cDNA templates were then used for qPCR using a LightCycler 480 DNA SYBR Green I Master kit (Roche) in the LightCycler 480 II system (Roche). The reaction conditions were as follows: Denaturation (95°C for 5 minutes), amplification was performed for 45 cycles (95°C for 10s, 60°C for 20s, 72°C for 10s) and a melt curve programme (65-95°C with a heating rate of 0.1°C/second). All primers were from Sigma and used at 0.3 µM. GAPDH was used as a control to normalize the data. GAPDH primers: 5′-GAAGCACCATGGAAAGGAAT-3′ (forward) and 5′-TCCTATAGCTGGGTGTTCCC-3′ (reverse). Mouse Bim primers: 5'-GTGCAATGGCTTCCATACGAC-3' (forward); 5'-GTCTTCAGCCTCGCGGTAAT-3' (reverse). Human HTT transgene primers: 5'- CTGCACGGCATCCTCTATGT-3' (forward); 5'- TGTTCACGCAGTGGGCTATT-3' (reverse). qPCR was performed in triplicate for each mouse sample and a relative quantification approach was performed using the $2^{-\Delta\Delta Ct}$ method.

DAB immunohistochemistry

mHTT staining. Striatal samples were fixed in 4% paraformaldehyde/ PBS for 24 hours, washed three times in PBS, and cryopreserved in 30% sucrose overnight at 4°C, followed by embedding and freezing in Optimal Cutting Temperature (OCT) compound ready for cryosecting. 8 nm sections were cut from each striatal sample using a Leica CM1860 UV cryostat. Tissue sections were washed in PBS to remove the OCT embedding medium. Endogenous peroxidase activity was quenched with 3% hydrogen peroxide in 100% methanol for 45 min at RT. Tissue staining was carried out with Vectastain Elite ABC-HRP Kit (Peroxidase, Universal, Vector Laboratories, PK-6200) according to manufacturer's instruction. Briefly, tissues were blocked with normal horse serum (NHS) in TBS with 0.1% Triton-X100 (TBS-T) for 1 hour at RT, followed by an additional 15 minute block with avidin and a 15 minute block with biotin (Avidin/biotin blocking kit, Vector Laboratories, SP-2001). MW1 primary antibodies were diluted in TBS-T containing 1% NHS and incubated with tissue sections overnight at 4°C (1:100). Following 3-time (10 min each time) washing in TBS, secondary antibodies were applied to the tissues in NHS-containing TBS-T followed by the incubation of avidin and biotinylated complex. 3,3'-diaminobenzidine tetrahydrochloride (DAB) peroxidase chromogen was used for immunoreactivity (Vector Laboratories, SK-4100) and the nuclei were stained with haematoxylin (Sigma). The tissue sections were cover-slipped with DPX mounting medium (Sigma) in preparation for bright field microscopy using a Leica IM8.

Cleaved caspase 3 staining. Cleaved caspase 3 (Cell signalling, #9661) was diluted in TBS-T (1:100) and incubated with tissue sections overnight at 4°C. Biotinylated universal secondary antibodies were diluted in TBS-T with 1% NGS. The avidin and biotinylated complex was applied as directed by the Vectastain Elite ABC-HRP Kit (Peroxidase, Standard, Vector Laboratories, PK-6200) and DAB was used for subsequent immunoreactivity. For quantification, 200-500 cells per animal were scored and analysed.

Mouse brain tissue lysates

Mouse striata were weighed and suspended in 10 volumes (w/v) of buffer A (20 mM Tris-HCl, pH 7.2, 2 mM $MgCl_2$, 150 mM NaCl, 0.5% NP-40, protease inhibitor cocktail [Roche]). The mixtures were incubated for 20 min on ice with swirling, and lysed by 15 strokes in a Dounce homogenizer. Equal amount of proteins (35 µg) were loaded for SDS-PAGE and immunoblot assays

Toluidine Blue staining

Tissue sections were washed in PBS for 5 minutes to remove the OCT embedding medium. Add 0.001% Toluidine blue dye (Fisher) to the tissue for 1 min at room temperature. Tissues were washed with distilled H_2O several times before serial immersion in 96% and 100% ethanol for 2 x 1 minute. Tissues were mounted with Citifluor mountant. LAS-X line profiling was used to quantify the staining levels. A threshold was set for the estimation of the cells with positive staining or negative staining. 200-500 cells per animal were scored and analysed.

Mouse behavioural and functioning assessment

We have identified the following five phenotypic tests that reliably discriminate between HD Bim+/+ mice, HD-tg Bim+/- or WT mice for mouse locomotor activity and behaviours. A minimal 9 of animals were used per genotype and time point.

Rotarod

Rotarod training and testing were performed on mice at 6, 8 10, 12, 14 and 16 weeks of age. Mice were placed onto a rotarod with an increasing ramp speed from 2 to 40 rpm in 250 seconds and the latency to fall (seconds) was recorded, as previously described (46, 47).

Grip strength

Grip strength testing was used to measure forelimb grip strength in control, HD or HD Bim+/- animals. Three grip strength trials were carried out prior to the tests. Animals were given at least 30-min rest between each trial. Each animal was lifted by the tail and slowly lowered down towards a horizontal metal bar. Upon grasping the bar, the animal was gently pulled backwards by the tail. Grip strength was manually assessed and a score of 0-2 was given: 0, no grip; 1, slight grip and; 2 active grip. An average score was given per genotype. Animals were tested in a randomized order and the assessor was blinded to previous trial scores (31).

Open-field test

The Open field test was carried out in a quiet and dimly lit room, using an opaque plastic box (400 mm x 400 mm x 400 mm). Mice were placed into the empty open field box for a duration of 5 min and left to explore the box; this was referred to as the habituation session for the novel object recognition test. A camera was placed overhead to record movement using NORT-3D tracking system (Bioseb, France). Each session was digitally recorded and the total distance travelled (cm) and global mean speed was analysed using the tracking system.

Novel object recognition test

Novel object recognition test (NORT) was used to evaluate memory, through the recognition of a previously explored object (familiar), compared to a novel object (unfamiliar). 24 hours after animals had been placed into the open field box for habituation, animals were individually placed into the same box now containing two identical (familiar) objects equally spaced apart. Animals were given 5 min to explore the two objects, and this is referred to as the familiarisation session. One hour later, animals were again individually placed back into the open field box, now containing one familiar object and one novel object. The animals

were left to explore the two objects for 5 min (this is referred to as the test session). Each session was digitally recorded, and a range of parameters including number of explorations at the familiar and novel object, total number of explorations and visit durations or numbers at the familiar and novel object, were analysed using the NORT-3D computer tracking system. Discrimination ratios were calculated using the formula: (Duration or visits at the novel object - Duration or visits at the familiar object) / (Duration or visits at the novel object + Duration or visits at the familiar object), as previously described (34).

Marble burying

Burying is a natural habit of mice. Marble burying is often used to depict changes in animal behaviour such as anxiety or obsessive-compulsive disorder. Here we analysed marble burying amongst mice at 6, 8, 10, 12 and 14 weeks of age. Animals were placed individually into a cage containing 12 glass marbles (1 cm), evenly distributed across the cage and on top of approximately 5 cm deep bedding, as previously described (35). The mice were given 30 min to explore the cage and then returned to their home cage. The number of marbles buried was then counted. A marble was considered buried if 2/3 or more was covered with bedding.

Quantification of autoradiographs

To quantify protein band density, the relevant specified bands were analysed using Image J software. The relative value was computed.

Statistical analysis

Statistical analysis was performed primarily with Graphpad Prism. The unpaired two-tailed t-tests were conducted for the comparison between two groups. One-way or two-way ANOVA tests were used for the comparison among multiple groups: one-way ANOVA for variables influenced by a single factor; two-way ANOVA for variables influence by two or more

factors (***, P<0.001, **, P<0.01, *, P<0.05, NS, not significant). T-tests were used for two-sample comparisons. Data from at least three independent experiments were analysed.

Acknowledgments

We are grateful to the Medical Research Council UK (MR/M023605/1) (SL), BRACE Charity (SL), Newton Advanced Fellowship (NAF\R1\191045) (SL & BL) for funding. We are grateful to Brain UK and the Cambridge Brain Bank (14/007) (supported by the NIHR Cambridge Biomedical Research Centre) for support.

Conflict of Interest Statement

The authors declare no conflict of interest.

References

1 Ross, C.A. and Tabrizi, S.J. (2011) Huntington's disease: from molecular pathogenesis to clinical treatment. *Lancet Neurol*, **10**, 83-98.

2 Walker, F.O. (2007) Huntington's disease. *Lancet*, **369**, 218-228.

3 (1993) A novel gene containing a trinucleotide repeat that is expanded and unstable on Huntington's disease chromosomes. The Huntington's Disease Collaborative Research Group. *Cell*, **72**, 971-983.

4 Yang, H., Liu, C., Zhong, Y., Luo, S., Monteiro, M.J. and Fang, S. (2010) Huntingtin interacts with the cue domain of gp78 and inhibits gp78 binding to ubiquitin and p97/VCP. *PLoS One*, **5**, e8905.

5 Zuccato, C., Valenza, M. and Cattaneo, E. (2010) Molecular mechanisms and potential therapeutical targets in Huntington's disease. *Physiol Rev*, **90**, 905-981.

6 Vonsattel, J.P., Keller, C. and Del Pilar Amaya, M. (2008) Neuropathology of Huntington's disease. *Handb Clin Neurol*, **89**, 599-618.

7 Feng, X., Luo, S. and Lu, B. (2018) Conformation Polymorphism of Polyglutamine Proteins. *Trends Biochem Sci*, **43**, 424-435.

8 Soto, C. (2003) Unfolding the role of protein misfolding in neurodegenerative diseases. *Nat Rev Neurosci*, **4**, 49-60.

9 Zhang, S., Binari, R., Zhou, R. and Perrimon, N. (2010) A genomewide RNA interference screen for modifiers of aggregates formation by mutant Huntingtin in Drosophila. *Genetics*, **184**, 1165-1179.

10 Baldo, B., Weiss, A., Parker, C.N., Bibel, M., Paganetti, P. and Kaupmann, K. (2012) A screen for enhancers of clearance identifies huntingtin as a heat shock protein 90 (Hsp90) client protein. *J Biol Chem*, **287**, 1406-1414.

11 Lu, B. and Palacino, J. (2013) A novel human embryonic stem cell-derived Huntington's disease neuronal model exhibits mutant huntingtin (mHTT) aggregates and soluble mHTT-dependent neurodegeneration. *FASEB J*, **27**, 1820-1829.

12 Yu, M., Fu, Y., Liang, Y., Song, H., Yao, Y., Wu, P., Yao, Y., Pan, Y., Wen, X., Ma, L. *et al.* (2017) Suppression of MAPK11 or HIPK3 reduces mutant Huntingtin levels in Huntington's disease models. *Cell Res*, **27**, 1441-1465.

13 Yao, Y., Cui, X., Al-Ramahi, I., Sun, X., Li, B., Hou, J., Difiglia, M., Palacino, J., Wu, Z.Y., Ma, L. *et al.* (2015) A striatal-enriched intronic GPCR modulates huntingtin levels and toxicity. *Elife*, **4**.

14 Tabrizi, S.J., Leavitt, B.R., Landwehrmeyer, G.B., Wild, E.J., Saft, C., Barker, R.A., Blair, N.F., Craufurd, D., Priller, J., Rickards, H. *et al.* (2019) Targeting Huntingtin Expression in Patients with Huntington's Disease. *N Engl J Med*, in press.

15 Saudou, F. and Humbert, S. (2016) The Biology of Huntingtin. *Neuron*, **89**, 910-926.

16 Puthalakath, H., Huang, D.C., O'Reilly, L.A., King, S.M. and Strasser, A. (1999) The proapoptotic activity of the Bcl-2 family member Bim is regulated by interaction with the dynein motor complex. *Mol Cell*, **3**, 287-296.

17 Puthalakath, H., O'Reilly, L.A., Gunn, P., Lee, L., Kelly, P.N., Huntington, N.D., Hughes, P.D., Michalak, E.M., McKimm-Breschkin, J., Motoyama, N. *et al.* (2007) ER stress triggers apoptosis by activating BH3-only protein Bim. *Cell*, **129**, 1337-1349.

18 Putcha, G.V., Moulder, K.L., Golden, J.P., Bouillet, P., Adams, J.A., Strasser, A. and Johnson, E.M. (2001) Induction of BIM, a proapoptotic BH3-only BCL-2 family member, is critical for neuronal apoptosis. *Neuron*, **29**, 615-628.

19 Luo, S., Garcia-Arencibia, M., Zhao, R., Puri, C., Toh, P.P., Sadiq, O. and Rubinsztein, D.C. (2012) Bim inhibits autophagy by recruiting Beclin 1 to microtubules. *Mol Cell*, **47**, 359-370.

20 Kong, P.J., Kil, M.O., Lee, H., Kim, S.S., Johnson, G.V. and Chun, W. (2009) Increased expression of Bim contributes to the potentiation of serum deprivation-induced apoptotic cell death in Huntington's disease knock-in striatal cell line. *Neurol Res*, **31**, 77-83.

21 Leon, R., Bhagavatula, N., Ulukpo, O., McCollum, M. and Wei, J. (2010) BimEL as a possible molecular link between proteasome dysfunction and cell death induced by mutant huntingtin. *Eur J Neurosci*, **31**, 1915-1925.

22 Ley, R., Balmanno, K., Hadfield, K., Weston, C. and Cook, S.J. (2003) Activation of the ERK1/2 signaling pathway promotes phosphorylation and proteasome-dependent degradation of the BH3-only protein, Bim. *J Biol Chem*, **278**, 18811-18816.

23 Bennett, E.J., Shaler, T.A., Woodman, B., Ryu, K.Y., Zaitseva, T.S., Becker, C.H., Bates, G.P., Schulman, H. and Kopito, R.R. (2007) Global changes to the ubiquitin system in Huntington's disease. *Nature*, **448**, 704-708.

24 Wang, J., Wang, C.E., Orr, A., Tydlacka, S., Li, S.H. and Li, X.J. (2008) Impaired ubiquitin-proteasome system activity in the synapses of Huntington's disease mice. *J Cell Biol*, **180**, 1177-1189.

25 Garcia-Martinez, J.M., Perez-Navarro, E., Xifro, X., Canals, J.M., Diaz-Hernandez, M., Trioulier, Y., Brouillet, E., Lucas, J.J. and Alberch, J. (2007) BH3-only proteins Bid and Bim(EL) are differentially involved in neuronal dysfunction in mouse models of Huntington's disease. *J Neurosci Res*, **85**, 2756-2769.

26 Schilling, G., Becher, M.W., Sharp, A.H., Jinnah, H.A., Duan, K., Kotzuk, J.A., Slunt, H.H., Ratovitski, T., Cooper, J.K., Jenkins, N.A. *et al.* (1999) Intranuclear inclusions and neuritic aggregates in transgenic mice expressing a mutant N-terminal fragment of huntingtin. *Hum Mol Genet*, **8**, 397-407.

27 Lu, B., Al-Ramahi, I., Valencia, A., Wang, Q., Berenshteyn, F., Yang, H., Gallego-Flores, T., Ichcho, S., Lacoste, A., Hild, M. *et al.* (2013) Identification of NUB1 as a

suppressor of mutant Huntington toxicity via enhanced protein clearance. *Nat Neurosci*, **16**, 562-570.

28 Bouillet, P., Metcalf, D., Huang, D.C., Tarlinton, D.M., Kay, T.W., Kontgen, F., Adams, J.M. and Strasser, A. (1999) Proapoptotic Bcl-2 relative Bim required for certain apoptotic responses, leukocyte homeostasis, and to preclude autoimmunity. *Science*, **286**, 1735-1738.

29 Gray, M., Shirasaki, D.I., Cepeda, C., Andre, V.M., Wilburn, B., Lu, X.H., Tao, J., Yamazaki, I., Li, S.H., Sun, Y.E. *et al.* (2008) Full-length human mutant huntingtin with a stable polyglutamine repeat can elicit progressive and selective neuropathogenesis in BACHD mice. *J Neurosci*, **28**, 6182-6195.

30 Hodgson, J.G., Agopyan, N., Gutekunst, C.A., Leavitt, B.R., LePiane, F., Singaraja, R., Smith, D.J., Bissada, N., McCutcheon, K., Nasir, J. *et al.* (1999) A YAC mouse model for Huntington's disease with full-length mutant huntingtin, cytoplasmic toxicity, and selective striatal neurodegeneration. *Neuron*, **23**, 181-192.

31 Ravikumar, B., Vacher, C., Berger, Z., Davies, J.E., Luo, S., Oroz, L.G., Scaravilli, F., Easton, D.F., Duden, R., O'Kane, C.J. *et al.* (2004) Inhibition of mTOR induces autophagy and reduces toxicity of polyglutamine expansions in fly and mouse models of Huntington disease. *Nat Genet*, **36**, 585-595.

32 Manfre, G., Clemensson, E.K.H., Kyriakou, E.I., Clemensson, L.E., van der Harst, J.E., Homberg, J.R. and Nguyen, H.P. (2017) The BACHD Rat Model of Huntington Disease Shows Specific Deficits in a Test Battery of Motor Function. *Front Behav Neurosci*, **11**, 218.

33 Rao, A.K., Gordon, A.M. and Marder, K.S. (2011) Coordination of fingertip forces during precision grip in premanifest Huntington's disease. *Mov Disord*, **26**, 862-869.

34 Galeano, P., Martino Adami, P.V., Do Carmo, S., Blanco, E., Rotondaro, C., Capani, F., Castano, E.M., Cuello, A.C. and Morelli, L. (2014) Longitudinal analysis of the

behavioral phenotype in a novel transgenic rat model of early stages of Alzheimer's disease. *Front Behav Neurosci*, **8**, 321.

35 Deacon, R.M. (2006) Digging and marble burying in mice: simple methods for in vivo identification of biological impacts. *Nat Protoc*, **1**, 122-124.

36 Ennaceur, A., Michalikova, S., Bradford, A. and Ahmed, S. (2005) Detailed analysis of the behavior of Lister and Wistar rats in anxiety, object recognition and object location tasks. *Behav Brain Res*, **159**, 247-266.

37 Sanchez, I., Mahlke, C. and Yuan, J. (2003) Pivotal role of oligomerization in expanded polyglutamine neurodegenerative disorders. *Nature*, **421**, 373-379.

38 Ona, V.O., Li, M., Vonsattel, J.P., Andrews, L.J., Khan, S.Q., Chung, W.M., Frey, A.S., Menon, A.S., Li, X.J., Stieg, P.E. *et al.* (1999) Inhibition of caspase-1 slows disease progression in a mouse model of Huntington's disease. *Nature*, **399**, 263-267.

39 Luo, S. and Rubinsztein, D.C. (2013) BCL2L11/BIM: a novel molecular link between autophagy and apoptosis. *Autophagy*, **9**, 104-105.

40 Skouta, R., Dixon, S.J., Wang, J., Dunn, D.E., Orman, M., Shimada, K., Rosenberg, P.A., Lo, D.C., Weinberg, J.M., Linkermann, A. *et al.* (2014) Ferrostatins inhibit oxidative lipid damage and cell death in diverse disease models. *J Am Chem Soc*, **136**, 4551-4556.

41 Zhu, S., Zhang, Y., Bai, G. and Li, H. (2011) Necrostatin-1 ameliorates symptoms in R6/2 transgenic mouse model of Huntington's disease. *Cell Death Dis*, **2**, e115.

42 Ferrante, R.J., Andreassen, O.A., Dedeoglu, A., Ferrante, K.L., Jenkins, B.G., Hersch, S.M. and Beal, M.F. (2002) Therapeutic effects of coenzyme Q10 and remacemide in transgenic mouse models of Huntington's disease. *J Neurosci*, **22**, 1592-1599.

43 Button, R.W., Roberts, S.L., Willis, T.L., Hanemann, C.O. and Luo, S. (2017) Accumulation of autophagosomes confers cytotoxicity. *J Biol Chem*, **292**, 13599-13614.

44 Luo, S., Vacher, C., Davies, J.E. and Rubinsztein, D.C. (2005) Cdk5 phosphorylation of huntingtin reduces its cleavage by caspases: implications for mutant huntingtin toxicity. *J Cell Biol*, **169**, 647-656.

45 Bouillet, P., Purton, J.F., Godfrey, D.I., Zhang, L.C., Coultas, L., Puthalakath, H., Pellegrini, M., Cory, S., Adams, J.M. and Strasser, A. (2002) BH3-only Bcl-2 family member Bim is required for apoptosis of autoreactive thymocytes. *Nature*, **415**, 922-926.

46 Roberts, S.L., Dun, X.P., Doddrell, R.D.S., Mindos, T., Drake, L.K., Onaitis, M.W., Florio, F., Quattrini, A., Lloyd, A.C., D'Antonio, M. *et al.* (2017) Sox2 expression in Schwann cells inhibits myelination in vivo and induces influx of macrophages to the nerve. *Development*, **144**, 3114-3125.

47 Saporta, M.A., Shy, B.R., Patzko, A., Bai, Y., Pennuto, M., Ferri, C., Tinelli, E., Saveri, P., Kirschner, D., Crowther, M. *et al.* (2012) MpzR98C arrests Schwann cell development in a mouse model of early-onset Charcot-Marie-Tooth disease type 1B. *Brain*, **135**, 2032-2047.

Legends to Figures

Figure 1. Bim upregulation correlates with p62 increases in HD mice

(A) Grade-III human HD or control post-mortem striatal (putamen) lysates were subjected to immunoblot with indicated antibodies. Control samples in order (age/gender): 72/F, 69/M, 67/M, 66/F, 52/M, 49/M; HD samples in order: 70/F, 68/M, 66/M, 59/M, 57/M, 55/M. Bim protein levels were quantified and normalised over loading control. n=6. Data are mean±SEM. Statistical analyses were performed by T-test. *: P=0.0310.

(B) The lysates of striatal tissues from WT (male) or N171-82Q transgenic HD mice (male) (10-17 weeks) were subjected to immunoblot by anti-Bim, p62 or GAPDH antibodies.

(C) The relative levels of Bim protein (HD vs WT) from 10 to 17-week mice were quantified. The mean of Bim/GAPDH in each WT group was set as 1, and the relative value of Bim/GAPDH in HD mice is shown. n=5 animals (for all ages/genotypes). 10W: 4 male (M)/1 female (F) mice for both WT and HD; 12W: 5M for both WT and HD; 14W: 4M/1F for both WT and HD; 17W: 5M for WT, and 4M/1F for HD. Data are mean±SEM. Statistical analyses were performed by two-way ANOVA with Bonferroni posttests. *: P<0.05 (10W); ***: P<0.001 (12W); ***: P<0.001 (14W); *: P<0.05 (17W). Note that quantification shows the relative levels of Bim (HD over age-matched WT control).

(D) qPCR for Bim mRNA levels was performed with mRNAs from the striata of WT or HD mice (10-17 weeks). The data show the relative values, as the mRNA levels in each WT group were set as 1. n=5 animals (for all ages/genotypes). 10W: 4M/1F for both WT and HD; 12W: 5M for both WT and HD; 14W: 4M/1F for both WT and HD; 17W: 5M for WT, and

4M/1F for HD. Data are mean±SEM. Statistical analyses were performed by two-way ANOVA with Bonferroni posttests. ns: not significant.

(E) The lysates of striata from WT or HD mice (14 weeks) were subjected to immunoblot with the indicated antibodies. n=3 mice (M). The relative protein levels (versus GAPDH) were quantified. The mean of each protein/GAPDH in each control group was set as 1. Data are mean±SEM. Statistical analyses were performed by two-way ANOVA with Bonferroni posttests. ***: P<0.001; *: P<0.05; ns: not significant.

Figure 2. Bim reduction alleviates mHTT neurotoxicity *in vivo*

(A) SK-N-SH cells were transfected with control or Bim siRNA. After 24 hours, the cells were split and transfected with with GFP-HTT-21Q or 72Q for further 24 hours. Over 80% transfection efficiency was confirmed, and cell viability was analysed. n=3. Data are mean±SEM. Two-way ANOVA with Bonferroni posttests was performed for the comparison. **: P<0.01; ns: not significant. Knockdown efficiency was confirmed by immunoblot.

(B) STHdh Q111 knockin striatal cells were transfected with control or Bim siRNA. After 24 hours, cells were treated with control or serum starvation for 24 hours. Cell viability was analysed (the viability of non-starved, control siRNA knockdown cells was set as 100%). n=3 biological replicates. Data are mean±SEM. Two-way ANOVA with Bonferroni posttests was performed for the comparison. ***: P<0.001; ns: not significant. Knockdown efficiency was confirmed by immunoblot.

(C) The lysates of striata from three WT, HD or HD Bim+/- mice (3M) (12 weeks) were subjected to immunoblot with Bim, cleaved caspase 3 (C-Casp3) and GAPDH antibody successively.

(D) The tissues of striata from the mice as indicated (12 weeks) were subjected to immunohistochemistry with cleaved caspase 3 (C-Casp3) antibody. Bar: 10 μm. Red arrows mark C-Casp3 positive neurons. The neurons positive for C-Casp3 were scored, and the percentage of the neurons is shown. n=4 mice (4M) (WT or HD), 5 mice (5M) (HD Bim+/-). 200-500 cells per animal were scored and analysed. Data are mean±SEM. Statistical analysis was performed by one-way ANOVA. Tukey's test was used for the comparison. *: $P<0.05$; ***: $P<0.001$.

(E) The tissues of striata WT, HD, or HD Bim+/- mice (12 weeks) as indicated were subjected to Toluidine blue staining. Note that darker neuronal staining (quantified by LAS-X line profiling) in HD mice indicates enhanced neuronal death. Bar: 25 μm. Data show the percentage of cells stained with dark toluidine blue. n=6 mice (5M/1F) (WT), 5 mice (5M) (HD) or 5 mice (5M) (HD Bim+/-). 200-500 cells per animal were scored and analysed. Data are mean±SEM. The statistical analysis was performed by one-way ANOVA. Tukey's test was used for the comparison. *: $P<0.05$; ***: $P< 0.0001$.

Figure 3. Bim knockdown reduces mHTT

(A) SK-N-SH cells were transfected with control or Bim siRNA. After 24 hours, the cells were split and transfected with with GFP-HTT-72Q for further 24 hours. Bar: 20 μm. Aggregate-positive cells were scored. n=3 biological replicates. Data are mean±SEM. T-test

was performed for the comparison. ***: P<0.001. Knockdown efficiency was confirmed by immunoblot.

(B) The tissues of striata from WT, HD or HD Bim +/- mice (at 10, 12, 14 weeks) were subjected to immunohistochemistry with MW1 (anti-expanded polyQ) antibody. Bar: 10 μm. The striatal neurons with mHTT aggregates>1.5 μm were scored, and the percentage of the neurons positive for the mHTT aggregates is shown. n=6 or 7. Statistical analysis was performed by one-way ANOVA and Tukey's test for the comparison. ***: P<0.001; **: P<0.01; *: P<0.05. Data show the size of mHTT aggregates (see the method).

(C) The lysates of striata from WT, HD or HD Bim+/- mice (12 weeks of age) were subjected to immunoblot with MW1, Bim and GAPDH antibodies.

Figure 4. Bim reduction mitigates Huntington's disease-associated phenotypes

(A) Rotarod test was performed in WT, HD or HD Bim+/- mice at indicated ages (6, 8, 10, 12 or 14 weeks). Data are mean±SEM. n numbers are indicated in the figure. The statistical analysis was performed by two-way ANOVA test. ***: P<0.0001; *: P=0.0181 (WT vs HD Bim+/-). Table S1 lists the details of mouse genders for this experiment.

(B) Grip strength test was performed in WT, HD or HD Bim+/- mice at the indicated ages. Data are mean±SEM. n numbers are indicated in the figure. The statistical analysis was performed by two-way ANOVA test. ***: P<0.001; **: P<0.01; *: P<0.05. Table S1 lists the details of mouse genders for this experiment.

(C-D) WT, HD or HD Bim+/- mice at the indicated ages were examined in the Open-field test. Total distance travelled (**C**) and global mean speed (**D**) were digitally recorded. Data are mean±SEM. n numbers are indicated in the figure. The statistical analysis was performed by two-way ANOVA test. (**C**): ***: P<0.0001 (WT vs HD); *: P=0.0349 (WT vs HD Bim+/-); ***: P=0.0008 (HD vs HD Bim+/-); (**D**) ***: P<0.0001; ***: P=0.0003 (WT vs HD Bim+/-). Table S1 lists the details of mouse genders for this experiment.

(E-F) Novel object recognition test was performed in WT, HD or HD Bim+/- mice at indicated ages. Discrimination ratios (reflecting the duration (**E**) and times (**F**) of contact with novel objects) are shown. Data are mean±SEM. n numbers are indicated in the figure. The statistical analysis was performed by two-way ANOVA test. In **E**, ***: P=0.0004 (WT vs HD); P=0.8711 (WT vs HD Bim+/-); ***: P=0.0009 (HD vs HD Bim+/-); in **F,** ***: P=0.0006 (WT vs HD); P=0.5787 (WT vs HD Bim+/-); *: P=0.0182 (HD vs HD Bim+/-). Table S1 lists the details of mouse genders for this experiment.

(G) The total number of explorations (the total number of visits to familiar and novel objects) by WT, HD or HD Bim+/- mice at indicated ages, was digitally recorded in the Novel object recognition test. Data are mean±SEM. n numbers are indicated in the figure. The statistical analysis was performed by two-way ANOVA test. ***: P<0.0001 (WT vs HD); **: P=0.0041 (WT vs HD Bim+/-); **: P=0.0054 (HD vs HD Bim+/-). Table S1 lists the details of mouse genders for this experiment.

(H) Marble burying test was used for the mice at indicated ages. Data are mean±SEM. n numbers are indicated in the figure. The statistical analysis was performed by two-way ANOVA test. ***: P<0.0001. Table S1 lists the details of mouse genders for this experiment.

Figure 5. Bim reduction mitigates the life expectancy in HD mice

(A) The survival curves were plotted in HD and HD Bim+/- mice. n=47 (HD mice); n=26 (HD Bim+/- mice). The statistical analysis was performed by the log-rank test. *: P=0.0174. X: the average lifespan. Data are mean±SEM. Table S1 lists the details of mouse genders for this experiment.

(B) The diagram shows that mHTT causes Bim upregulation and neurotoxicity, and reduction in Bim alleviates cell death, thereby ameliorating mHTT toxicity.

Abbreviations

ASOs: antisense oligonucleotides

ER: endoplasmic reticulum

F: female

HD: Huntingtin's disease

HTT: huntingtin

HTT-21Q: HTT exon1-21Q

HTT-72Q: HTT exon1-72Q

mHTT: mutant HTT

polyQ: polyglutamine

M: male

NORT: Novel object recognition test

UPS: ubiquitin proteasome system

WT: wild-type

Fig. 1

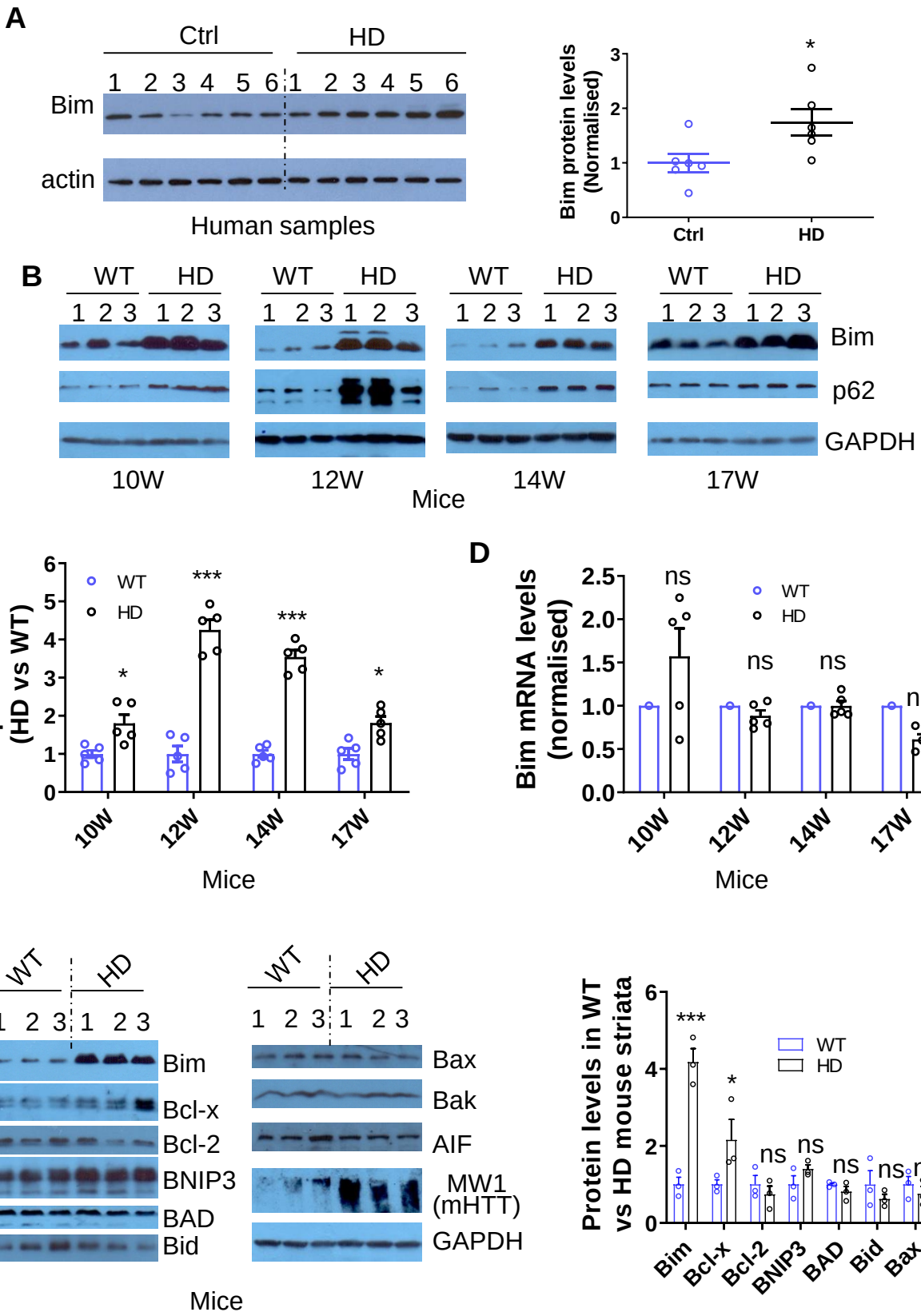
A
Ctrl
HD
1 2 3 4 5 6 1 2 3 4 5 6
Bim
actin
Human samples
Bim protein levels (Normalised)
Ctrl
HD
B
WT
HD
1 2 3
Bim
p62
GAPDH
10W
12W
14W
17W
Mice
C
Bim protein levels (HD vs WT)
WT
HD
10W
12W
14W
17W
Mice
D
Bim mRNA levels (normalised)
ns
WT
HD
Mice
E
Bim
Bcl-x
Bcl-2
BNIP3
BAD
Bid
Bax
Bak
AIF
MW1 (mHTT)
GAPDH
Mice
Protein levels in WT vs HD mouse striata
Bim
Bcl-x
Bcl-2
BNIP3
BAD
Bid
Bax
Bak
AIF

Fig. 2

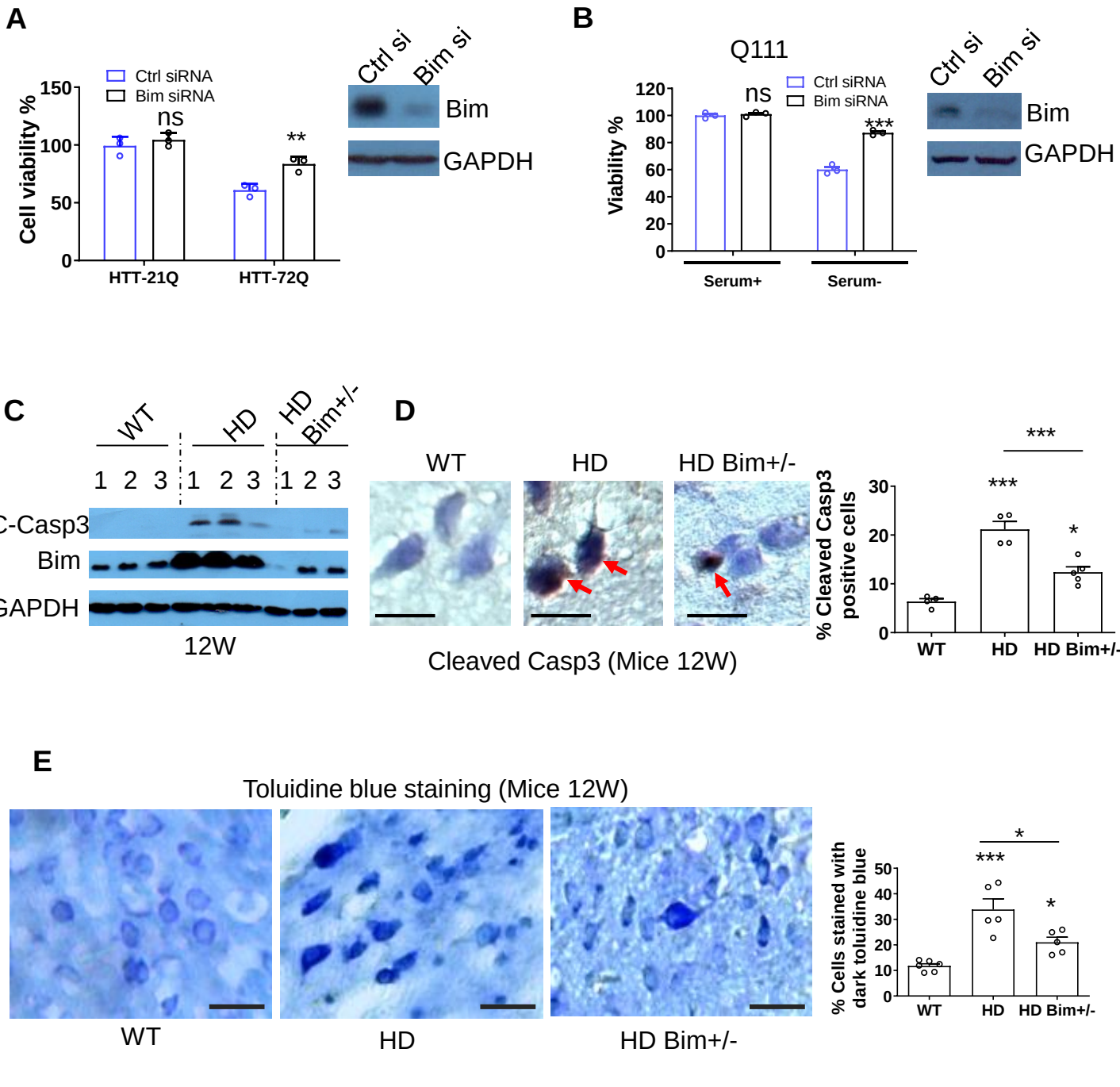
A
Cell viability %
150
100
50
0
Ctrl siRNA
Bim siRNA
ns
**
HTT-21Q
HTT-72Q
Ctrl si
Bim si
Bim
GAPDH
B
Q111
Viability %
120
100
80
60
40
20
0
Ctrl siRNA
Bim siRNA
ns
***
Serum+
Serum-
Ctrl si
Bim si
Bim
GAPDH
C
WT
HD
HD Bim+/-
1 2 3 1 2 3 1 2 3
C-Casp3
Bim
GAPDH
12W
D
WT
HD
HD Bim+/-
Cleaved Casp3 (Mice 12W)
% Cleaved Casp3 positive cells
30
20
10
0
***
***
*
WT
HD
HD Bim+/-
E
Toluidine blue staining (Mice 12W)
WT
HD
HD Bim+/-
% Cells stained with dark toluidine blue
50
40
30
20
10
0
*
***
*
WT
HD
HD Bim+/-

Fig. 3

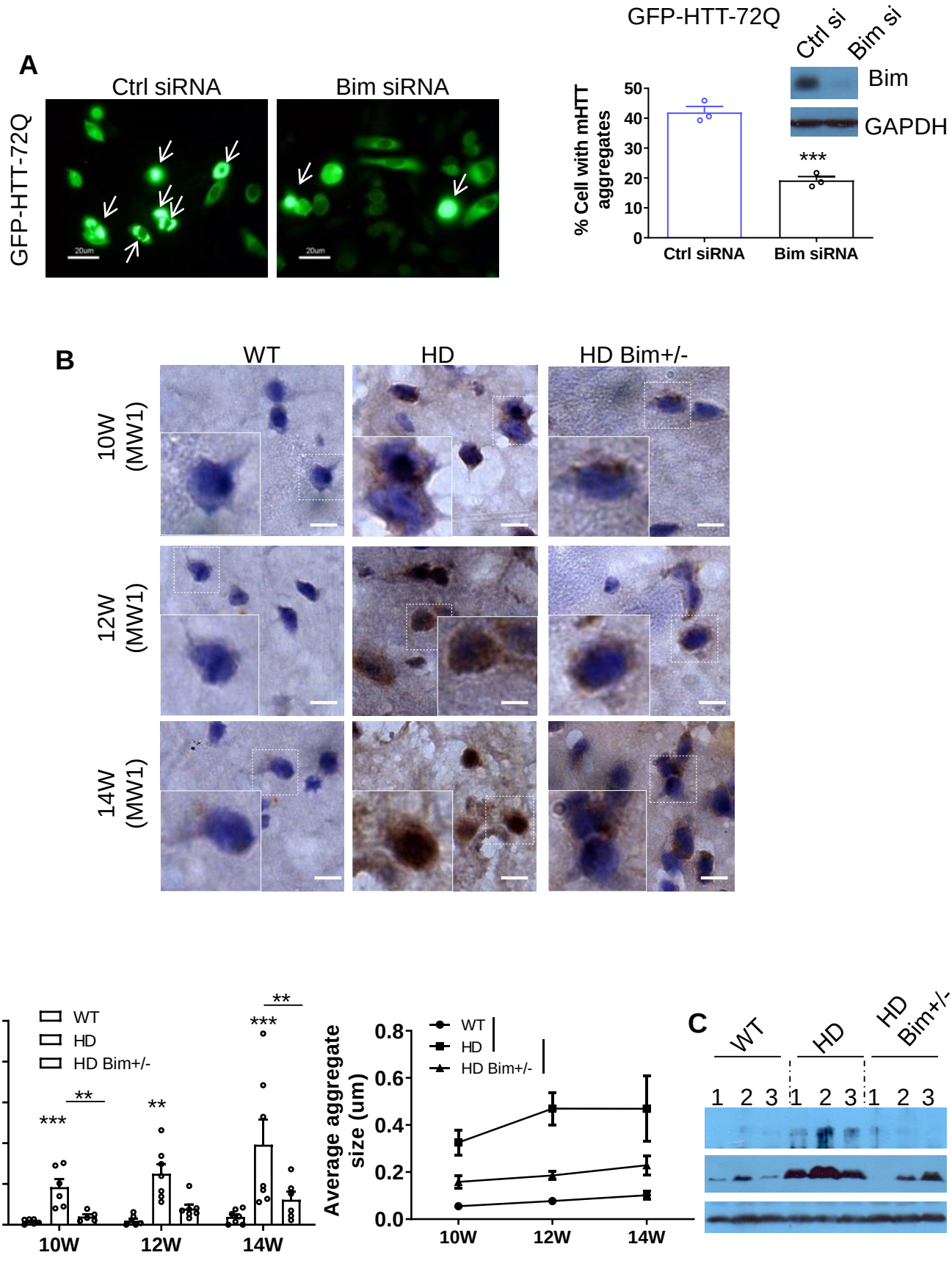
A
Ctrl siRNA
Bim siRNA
GFP-HTT-72Q
20um
GFP-HTT-72Q
Ctrl si
Bim si
Bim
GAPDH
% Cell with mHTT aggregates
50
40
30
20
10
0
***
Ctrl siRNA
Bim siRNA
B
WT
HD
HD Bim+/-
10W (MW1)
12W (MW1)
14W (MW1)
% of nuclei with mHTT aggregates >1.5um
WT
HD
HD Bim+/-
**
***
**
**
***
**
10W
12W
14W
Average aggregate size (um)
0.8
0.6
0.4
0.2
0.0
C
WT
HD
HD Bim+/-
1 2 3 1 2 3 1 2 3

Fig. 4

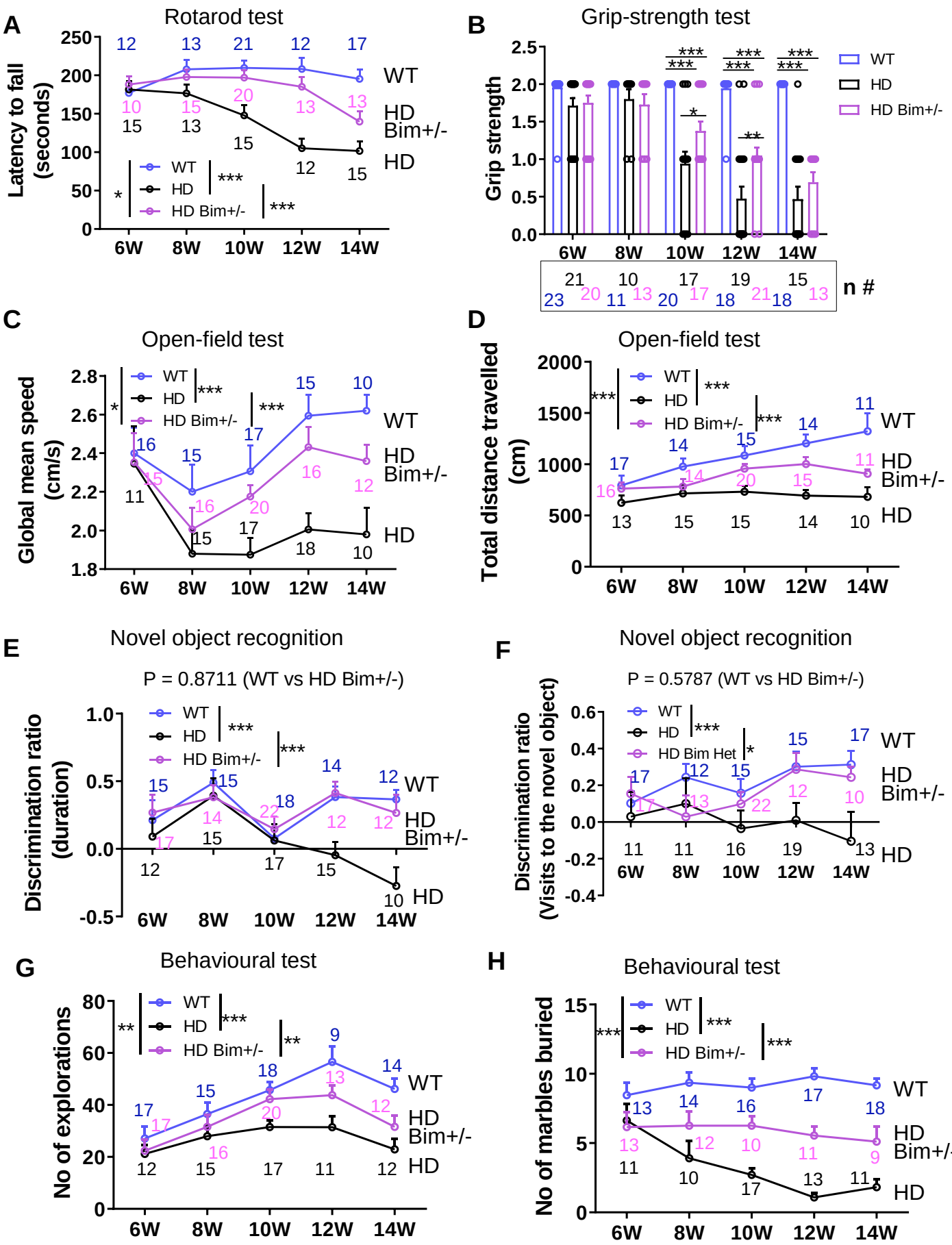
A
Rotarod test
Latency to fall (seconds)
WT
HD
HD Bim+/-
6W
8W
10W
12W
14W
B
Grip-strength test
Grip strength
n #
C
Open-field test
Global mean speed (cm/s)
D
Open-field test
Total distance travelled (cm)
E
Novel object recognition
P = 0.8711 (WT vs HD Bim+/-)
Discrimination ratio (duration)
F
Novel object recognition
P = 0.5787 (WT vs HD Bim+/-)
Discrimination ratio (Visits to the novel object)
HD Bim Het
G
Behavioural test
No of explorations
H
Behavioural test
No of marbles buried

Fig. 5

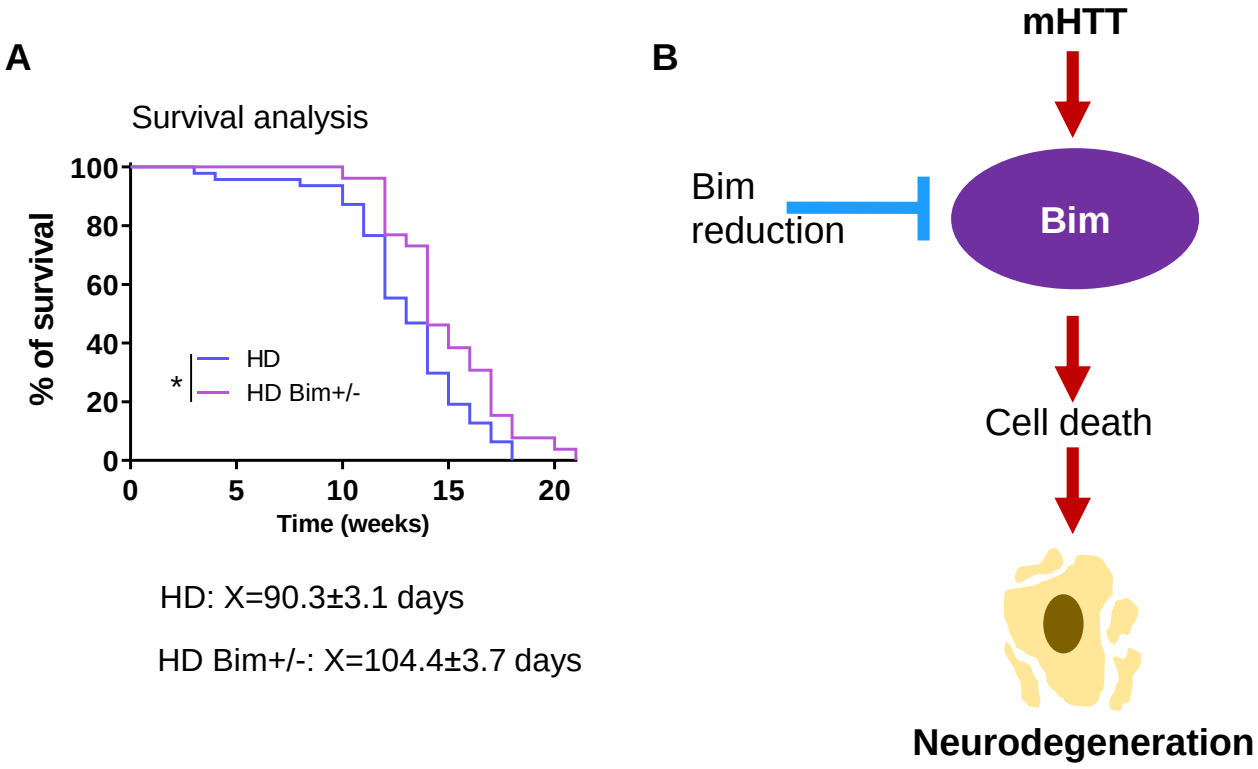
A
Survival analysis
% of survival
100
80
60
40
20
0
0
5
10
15
20
Time (weeks)
*
HD
HD Bim+/-
HD: X=90.3±3.1 days
HD Bim+/-: X=104.4±3.7 days
B
mHTT
Bim
reduction
Bim
Cell death
Neurodegeneration